Biophysical Journal Volume 95 September 2008 3009–3016

Localized Acetylcholine Receptor Clustering Dynamics in Response to Microfluidic Focal Stimulation with Agrin

Anna Tourovskaia, Nianzhen Li, and Albert Folch
Department of Bioengineering, University of Washington, Seattle, Washington

ABSTRACT Agrin is a proteoglycan secreted by the motor neuron's growing axon terminal upon contact with the muscle during embryonic development. It was long thought that agrin's role was to trigger the clustering of acetylcholine receptors (AChRs) to nascent synapse sites. However, agrin-predating, protosynaptic AChR clusters are present well before innervation in the embryo and in myotube cultures, yet no role has been conclusively ascribed to agrin. We used a microfluidic device to focally deliver agrin to protosynaptic AChR clusters in micropatterned myotube cultures. The distribution of AChRs labeled with fluorescent bungarotoxin was imaged at various time points over >24 h. We find that a 4-h focal application of agrin (100 nM) preferentially reduces AChR loss at agrin-exposed clusters by 17% relative to the agrin-deprived clusters on the same myotube. In addition, the focal application increases the addition of AChRs preferentially at the clusters by 10% relative to the agrin-exposed, noncluster areas. Taken together, these findings suggest that a focal agrin stimulus can play a key stabilizing role in the aggregation of AChRs at the early stages of synapse formation. This methodology is generally applicable to various developmental processes and cell types, including neurons and stem cells.

INTRODUCTION

Proper development of the nervous system relies on the delicately coordinated formation of synapses (1), which must occur at precise locations and times. Experimental interrogation of the synaptogenesis process in vivo is extremely difficult. Because genetic engineering of key molecules is often embryonically lethal and physical access to the synaptic site can disrupt synapse formation irreversibly. Even the formation of the neuromuscular synapse, the best studied synapse due to its relatively straightforward anatomical accessibility (1), is still not fully understood. In general, in vitro studies of embryonic development face great technological challenges, as development is a highly dynamic process that involves myriad signaling factors varying across subcellular length scales and at subminute timescales. Microtechnologies such as microfluidics and surface patterning offer a great potential for recreating physiological conditions by delivering signaling factors to the cells in physiologically meaningful spatial distributions and at a precise differentiation state. We have developed a microdevice that allows us to partially mimic the innervation of a muscle cell by a neuron.

A functional neuromuscular synapse consists of a high postsynaptic density of acetylcholine receptors (AChRs) (2). A highly dynamic AChR clustering mechanism, initiated during development, keeps the synaptic surface density of AChRs several orders-of-magnitude higher than at the extrasynaptic sites (2,3); AChRs form aggregates at nerve-contacted sites as well as spontaneously (4,5), and AChRs that do not associate with the nerve terminal eventually disappear (6–9). It was long thought that AChR clustering at the nascent synapse was triggered by the proteoglycan agrin (the agrin hypothesis (10)), which is secreted by the nerve terminal upon and/or during innervation (2,10,11) (Fig. 1 *A*). Unfortunately, in vivo it is not possible to artificially stimulate AChR clusters with agrin focally due to diffusion.

The observation that traditional myotube cultures form punctate microclusters of AChRs upon bath or focal application of agrin or an agrin fragment (see Fig. S1, *A* and *B*, in Supplementary Material) was thought to be supportive of the agrin hypothesis. Past efforts to mimic in vitro the nerve's local delivery of agrin have used focal stimulation with beads (12), agrin micropatterns (13), or co-cultures with agrin-producing cells (12), but could not (or did not) address protosynaptic AChR clusters (12,13) and could not control the location and/or timing of the focal stimulus (7,12,13). In the past, we have reported a microfluidic device that uses laminar flow to locally deliver biochemicals to a user-selected portion of an array of single myotubes cultured orthogonally to the flow (14,15). Focal agrin stimulation of myotubes seeded on fibronectin surfaces resulted in formation of microclusters in the stimulated areas, both in micropatterned (16) as well as in randomly-oriented myotubes (17) seeded on fibronectin surfaces.

Recently, however, imaging of embryos (both in mouse (18–20) and Zebrafish (8,21)) has revealed that large protosynaptic AChR aggregates of normal synaptic morphology form on the muscle membrane before the arrival of the nerve (Fig. 1 *A*). MuSK, a receptor tyrosine kinase activated by agrin, is required for the formation of the protosynaptic AChR clusters even though agrin is not (18). What is, then, the role of agrin, given that it is not the cause of AChR clustering? One possibility is that it acts to stabilize the existing clusters (although the nerve can also make synapses in

Submitted December 22, 2007, and accepted for publication April 25, 2008.

Address reprint requests to Albert Folch, Tel.: 206-685-2257; E-mail: afolch@u.washington.edu.

Editor: Denis Wirtz.

0006-3495/08/09/3009/08 $2.00

doi: 10.1529/biophysj.107.128173

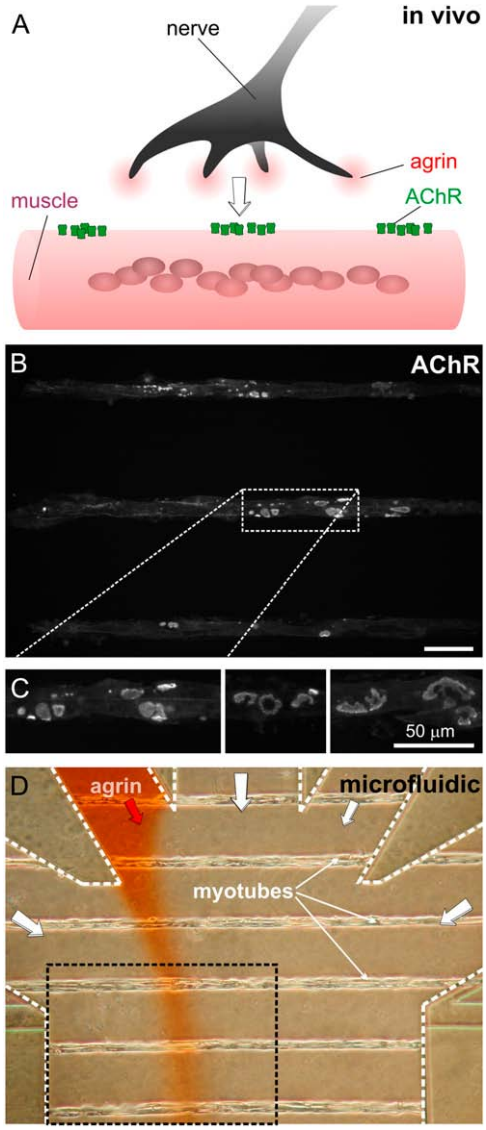

FIGURE 1 Synaptogenesis on a chip. (*A*) During development, neurons release agrin at the site of contact between nerve and muscle. (*B*) Fluorescence micrograph of a portion of the myotube microarray after staining the AChRs with Alexa Fluor 488-conjugated α-bungarotoxin (BTX*). Scale bar is 50 μm. (*C*) Three high-magnification fluorescence micrographs of myotubes stained with BTX*, showing that aneural AChR clusters display intricate shapes similar to those found in vivo. (*D*) Phase-contrast micrograph of the microfluidic device containing a ladder micropattern of myotubes during stimulation by a laminar stream of agrin (spiked with red Allura dye for visualization). The black-dashed box corresponds to the area shown in panel *B*.

regions where aneural AChR clusters do not form (5)). In support of this hypothesis, the agrin-predating protosynaptic clusters are stabilized if found by the nerve but dissolve if not innervated. An additional role of agrin appears to be to counteract the declustering action of acetylcholine (ACh), since synapses form in the absence of agrin provided that ACh is also absent (7). While these results add to challenge the agrin hypothesis, they do not conclusively attribute any specific synaptogenic role to agrin. Here we sought to address the fundamental question of how protosynaptic AChR clusters evolve upon local exposure to soluble agrin.

We used a microdevice to interrogate how, in the absence of neurotransmitter action, agrin-predating AChR clusters evolve upon local exposure to agrin in myotube cultures. After fluorescently labeling the AChR clusters, the fluorescence stability of agrin-exposed and agrin-deprived domains is compared. We observe that a short (4 h) focal application of agrin slows down the loss of AChRs from those clusters relative to the agrin-deprived clusters. Based on one relabeling at the end of the experiment (24–25 h), we observe that AChR addition is highest at the agrin-exposed clusters. Thus, agrin, at least in vitro, acts to selectively reduce and increase AChR loss and addition, respectively.

MATERIALS AND METHODS

Microfluidic device

Standard soft lithographic techniques were used to fabricate the device in poly(dimethylsiloxane) (PDMS) by replica molding from a microfabricated master; the design, fabrication, and operation of the device is described in detail elsewhere (14). The glass substrate was chemically micropatterned to restrict the areas available for cell attachment and myotube formation (22). Micropatterns of cell-adhesive tracks (PDL/Matrigel on glass) separated by a cell-repellent graft of polyethylene glycol were prepared using oxygen plasma etching and PDMS microchannels as masks, as reported previously (15,22).

Microfluidic myotube microarray culture

Microfluidic long-term cultures of micropatterned myotubes are described in detail elsewhere (19,23). Briefly, C2C12 myoblasts (ATCC, Manassas, VA) were cultured in tissue culture grade dishes before passage 10 in DMEM (Life Technologies, Bethesda, MA), supplemented with 20% fetal bovine serum (HyClone, Logan, UT) and 1% penicillin-streptomycin (Life Technologies), and maintained in a humidified incubator at 37°C with 10% CO_2. The cell suspension was injected into the microfluidic devices at ~2,000,000 cells/mL, and cells were allowed to attach and spread on the Matrigel-coated microtracks for 15–30 min before continuous perfusion from side channels was established. Fusion into myotubes was promoted at confluence (the day after seeding) by low-serum differentiating medium (DM) consisting of 5% horse serum (ATCC) and 1% penicillin-streptomycin-fungizone in DMEM. Myotubes formed in the device within 1 week after switching to DM.

Agrin stimulation

Localized stimulation was performed as discussed in detail elsewhere (14,15). Agrin (C-terminal fragment, C-$Ag_{3,4,8}$) was purchased from R&D Systems (Minneapolis, MN) and used at 100 nM final concentration. In localized-agrin experiments four laminar flow streams (three carrying DM and one carrying 100 nM agrin in DM) were flowed through the device at a velocity of 240 μm/s for 4 h. Shear stresses associated with such velocities were not observed to noticeably affect C2C12 cell viability, morphology, growth, or differentiation (15). After agrin flow was stopped, cells were washed and incubated in agrin-free medium over two days and imaged at selected time points (Fig. 2 *A*). Agrin flow was visualized during the experiment by adding Allura Red food dye (1 μg/ml) in the agrin-containing stream. We have not observed any obvious deleterious effects derived from the exposure of the myotubes to Allura at that concentration. Allura also had no AChR-aggregating effect (15,16). Because

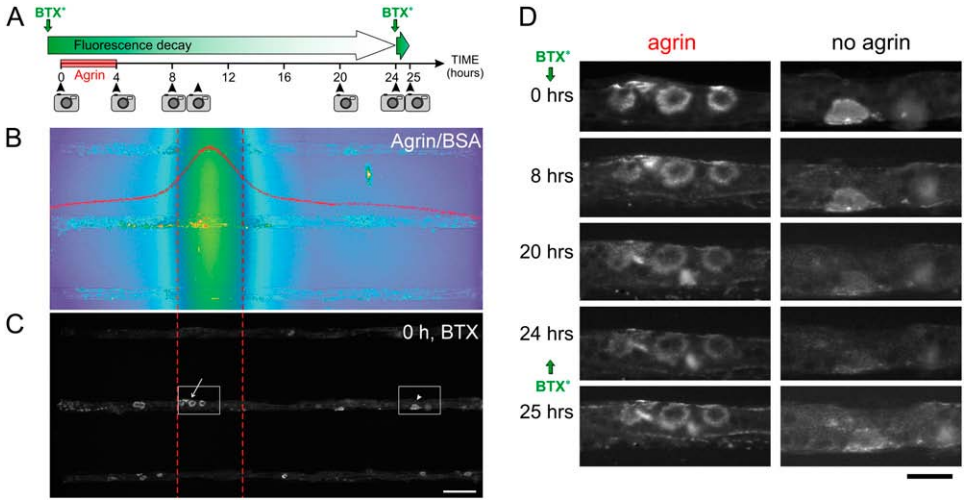

FIGURE 2 Focal application of agrin onto aneural AChR clusters. (*A*) Schematic of the experimental design showing the application of fluorescent AChR label (BTX*, *green vertical arrows*) and of agrin with the imaging times (camera icons). (*B*) Fluorescence micrograph (*false color*) of the stream of a fluorescent agrin tracer (Texas Red-conjugated BSA) taken at the end of the experiment, which serves to extrapolate the agrin concentration profile (see Data S1). Overlaid is a line scan (*red curve*) across the micrograph; clusters are considered exposed to agrin if they are in an area exposed to at least 10% of the maximal agrin concentration, and agrin-deprived otherwise. For reference, red dashed lines denote 50% of maximal agrin concentration. (*C*) Fluorescence BTX* staining of the same area as in panel *B*, showing three myotubes across the device. Scale bar is 50 μm. (*D*) Time evolution of the two areas boxed in panel *C* from the same myotube. The myotubes were labeled with BTX* right before $t = 0$ h and right after the $t = 24$ h time-point image. Cells were focally exposed to agrin (0–4 h) and imaged at the indicated time points. Scale bar is 25 μm.

fluorescent tagging of agrin is not practical and could affect agrin signaling, we quantified the agrin (molecular mass ~90 kDa) profile using fluorescently-conjugated BSA (Texas Red BSA, molecular mass ~70 kDa) (BSA*) at the end of each experiment. The width of the agrin stream during focal stimulation can be inferred from the width of the BSA* stream (Fig. 2 *B*) because the diffusion coefficient D is insensitive to changes in molecular weight, $D \sim (\mathrm{MW})^{-1/3}$, and the mean diffusive path x is not very sensitive to changes in D ($x \sim D^{-1/2}$) (24). AChR clusters that fell within >10% of the BSA* peak intensity were considered to be agrin-exposed and the clusters that fell outside of that area were considered to be agrin-deprived.

Imaging

Fluorescence and phase-contrast images were acquired on an inverted microscope (Nikon Eclipse TE2000-U; Nikon, Melville, NY) with a cooled charge-coupled device camera (ORCA-HR; Hamamatsu Photonics, Hamamatsu City, Japan) using commercial imaging software (MetaMorph; Universal Imaging, Downingtown, PA). Care was taken to minimize the photobleaching by keeping illumination intensity at low levels. Exposure times, camera offset, and gain settings were kept constant for all images on all days. To cover the entire channel width, two overlapping images were taken (a few seconds apart) at each time point and processed separately. There are ~60 myotubes per device, of which we only consider the upstream two-thirds for analysis, to avoid confounding effects by agrin stream broadening downstream. The microscope's field of view fits only three half-myotubes, so for each experiment 14 pairs of side-by-side images were acquired, each pair spanning in width the length of a myotube (i.e., the width of the device). Thus, each experiment yielded data on ~42 myotubes. Only myotubes with clusters on the agrin-exposed areas were chosen for analysis ($N = 23$, $N = 15$, and $N = 10$ for experiments 1, 2, and 3). The cells were returned to a standard tissue culture incubator after each imaging session.

Labeling of cells

Myotubes were labeled with Alexa 488-conjugated α-bungarotoxin (BTX*) at 5 μg/ml for 1 h to saturate all AChRs (25), washed in phenol red-free DM, and imaged (time-point 0 h). Cells were then exposed to agrin for 4 h, washed, and imaged again (time-point 4 h). Finding the same area was straightforward because cells were arranged in micropatterns. The cells were reimaged again at 8, 10, 20, and 24 h (Fig. 2 *A*). Finally, after taking the 24-h time-point image, the AChRs were relabeled to saturation and the cells were reimaged 1 h (25-h time-point) later to assess the total AChR density. We also assessed the rate of photobleaching of BTX* bound to the AChR clusters. Labeled myotubes were fixed, imaged, and immediately reimaged; the fluorescence loss resulting from photobleaching was found to be <1% between sequential images. In principle, we cannot rule out the possibility that (labeled) internalized AChRs or (unquenched) free Alexa dye (from degraded AChRs) in the cytoplasm contribute to the fluorescence intensity of the myotube (i.e., both nonclustered and clustered AChR areas) and partially confound AChR distribution changes. However, since the clusters occupy only ~6–7% of the myotube membrane, and the density in the clusters is at the most only ~3 times that of the noncluster areas, internalized clustered receptors (which, in addition, go out of focus) are unlikely to contribute significantly to the fluorescence signal. Also, the fluorescence of Alexa 488 (that is, stable at lysosomal pH) can be quenched by denaturing BTX (26). In any case, the cellular origin of the background fluorescence is relevant to the measurements of the stability of noncluster areas but is irrelevant to the conclusion that agrin reduces the loss and increases the addition of AChRs at cluster areas relative to their surroundings. See Data S1 in Supplementary Material for a detailed explanation of the image analysis.

RESULTS

Microfluidic focal agrin stimulation

As a quantitative model of the selective exposure of the myotube membrane to agrin in vivo (Fig. 1 *A*), we have developed a microfluidic device that delivers agrin selectively to a user-selected portion of an array of >60 single, parallel myotubes cultured orthogonally to the flow (14). We use a well-characterized in vitro model of muscle cell differentiation based on C2C12 myoblast cultures, which fuse to form functional myotubes (27,28). We use the recombinant C-terminal neural agrin fragment, which is known to potently induce punctate AChR clusters in myotube cultures under bath (29) and focal (16) application.

Before agrin delivery, isolated myotubes already display several (~8 ± 5.5 per myotube) intricately-shaped proto-

synaptic AChR clusters as revealed by the permanent AChR label α-bungarotoxin (BTX) conjugated with Alexa Fluor 488 (BTX*). As shown in Fig. 1, *B* and *C*, AChR clusters of complex morphologies (strikingly similar to those found in vivo) can, too, form in vitro in the absence of agrin if the myotubes are cultured on micropatterns of the basal lamina extract Matrigel (Fig. S1, *C* and *D* for diversity of morphologies), whether inside or outside a device. Nonmicropatterned myotubes also display agrin-independent AChR clusters on Matrigel (Fig. S1 *E*) and on laminin (23,30), but not on a fibroblast feeder layer (Fig. S1 *F*).

The device is fabricated by micromolding of a transparent elastomer, PDMS, and assembled onto an array of 25 μm-wide linear tracks of dried Matrigel on glass that are separated by a polyethylene-glycol graft nonadherent to cells (15,22). As a result, C2C12 cells introduced inside the device proliferate and fuse (over ~1 week) into myotubes only on the Matrigel tracks, forming a ladder of single myotubes (Fig. 1 *D*) (14). Only one of the inlets is filled with agrin, so that under laminar flow conditions typical of microchannels (i.e., no turbulence), the fraction of each myotube exposed to a given concentration of agrin can be inferred from the spatial distribution of a dye added to the agrin solution (16) (see below).

As shown in the Fig. 2 *A* schematic, in a typical experiment the myotubes were:

1. Labeled with BTX* and immediately imaged, which defined time $t = 0$.
2. Exposed to agrin from 0 to 4 h.
3. Imaged by fluorescence microscopy at $t = 4$, 8, 10, 20, and 24 h.
4. Relabeled at 24 h to assess the addition of new AChRs; and
5. Imaged at 25 h.

The agrin stream's position was visualized during the experiment by adding to the agrin-containing stream a food-coloring dye (Allura Red, 1 μg/ml) (Fig. 1 *D*), and the concentration profile was measured after the experiment by adding fluorescently-labeled bovine serum albumin (BSA) (of diffusivity similar to that expected of agrin; see Data S1) (Fig. 2 *B*). Fig. 2 *C* shows the BTX*-staining of the same area of the device as in Fig. 2 *B*, revealing some clusters in the agrin path and some outside of it. We have not observed deleterious or AChR-aggregating effects derived from the exposure of the myotubes to the dyes alone at the concentrations used (16). The concentration profile widens diffusively downstream (with no discernible effect on the conclusions of this study, see Fig. S3; only the upstream two-thirds of the device are used for analysis). For simplicity of analysis, agrin exposure is considered binary, i.e., exposed to agrin (if exposed to at least 10% of the maximal agrin concentration, or 100 nM at inlet) or deprived of agrin (otherwise). A typical time sequence of agrin-exposed and agrin-deprived (BTX*-stained) clusters is shown in Fig. 2 *D* (*left* and *right columns*, respectively).

To measure AChR density, four types of regions are identified and manually selected in each myotube, as shown schematically in Fig. 3 *A*: regions *A* and *C* correspond to AChR cluster areas exposed to and deprived of agrin, respectively, whereas regions *B* and *C* correspond to the myotube membrane background (adjacent to regions *A* and *C*) exposed to and deprived of agrin, respectively. The average fluorescence intensity of each region is recorded over time and background-corrected (Fig. S2), giving time functions $A(t)$, $B(t)$, $C(t)$, and $D(t)$ for each myotube. Photobleaching and BTX* binding to other components of the membrane or the substrate are negligible in our fluorescence imaging setup, and the potential contribution from free fluorophore in the cytoplasm (after BTX*-AChR internalization and degradation) can be ruled out (see Data S1); therefore, the fluorescence intensity after background correction is approximately proportional to AChR density.

Focal agrin slows down AChR loss at agrin-predating clusters

AChR density changes as a function of time can be qualitatively assessed from the averages $A(t)$, $B(t)$, etc., as shown in Fig. 3 *B* from a representative experiment ($N = 23$ myotubes, ~184 clusters). The AChR cluster areas $A(t)$ and $C(t)$ are initially ~3 times brighter than their neighboring noncluster areas $B(t)$ and $D(t)$, and over time the clusters fade (a sign of AChR internalization and degradation (31)) while the noncluster areas remain approximately constant. (See Materials and Methods and Data S1for the various contributions to the fluorescence signal, including diffuse and internalized receptors or cytoplasmic Alexa dye.) The rate of decay for $A(t)$ and $C(t)$ tapers off (~60% of the agrin-exposed and ~40% of the agrin-deprived AChRs in the clusters still remain at $t = 24$ h), which hints at a density-dependent AChR loss process yielding an exponential decay (i.e., governed by Michaelis-Menten kinetics). However, the large variability in the $A(t)$, $B(t)$, etc. makes it difficult to ascertain more precise conclusions from this graph.

A more quantitative analysis can be done by averaging all the values of the ratios of the $A(t)$, $B(t)$, etc., for each myotube, thus using each region as a reference point for measuring another region's fluorescence; this ratiometric analysis based on cellular-scale, internal controls is insensitive to variations in the fluorescence excitation lamp or in background myotube membrane fluorescence. The summary of the ratiometric analysis for $n = 3$ experiments ($N = 48$ myotubes, ~384 clusters) is shown in Fig. 3, *C* and *D*. The data from the separate experiments is shown in different symbols (*circles*, *triangles*, *squares*) to emphasize that the trends are almost exact in each experiment. In other words, the error bars can be attributed mostly to variability from experiment to experiment, likely due to the accuracy of the ratiometric method. Fig. 3 *C* confirms that AChR density is ~3 times larger and less stable in cluster areas than in noncluster areas (i.e., both $A(t)/B(t)$ and

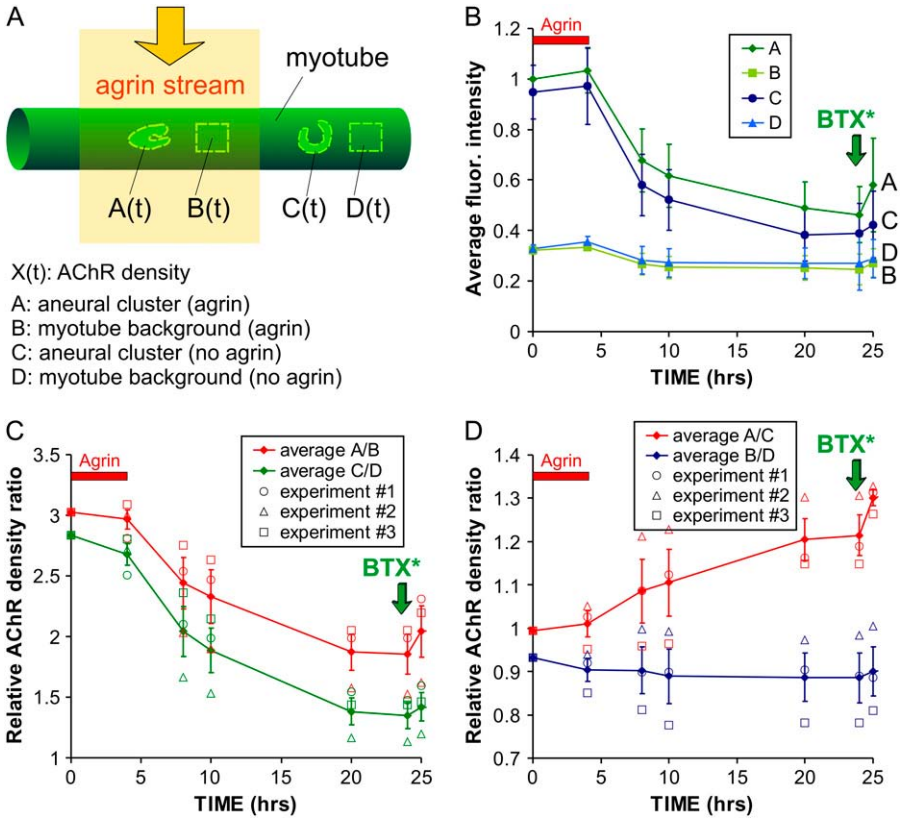

FIGURE 3 Local AChR density dynamics. (*A*) Schematic representation of the four regions that are defined and marked for analysis: cluster(s) and myotube background exposed to agrin (regions *A* and *B*, respectively) and cluster(s) and myotube background not exposed to agrin (*C* and *D*, respectively); *A* and *C* are typically comprised of several (range 2–16, average 8 ± SD 5.5) individual clusters. After labeling with a saturating dose of BTX* and background correction, fluorescence intensity in a region *X* (X = *A*, *B*, *C*, or *D*) is assumed to be proportional to AChR density, termed *X*(*t*). (*B*) Graph of the average fluorescence intensities in regions *A*–*C* and (values relative to the average *A*(0) for all myotubes) in a representative experiment containing $N = 23$ myotubes. BTX* was reapplied after $t = 24$ h (*green vertical arrows*) to visualize the total AChR density and to assess AChR addition (the $t = 24$ h data point for experiment 3 could not be obtained, so it was conservatively taken to be equal to the $t = 20$ h data point, despite the additional 4 h of degradation; this results in a lower estimate of AChR addition upon relabeling). (*C*) AChR density ratios (as indicated) as a function of time for $n = 3$ experiments (total $N = 48$ myotubes).

C(*t*)/*D*(*t*) are ~3 at $t = 0$ and decay thereafter). By $t = 20$–24 h, the agrin-exposed cluster areas *A*(*t*) are 21 ± 5% on average brighter than the agrin-deprived cluster areas *C*(*t*) (Fig. 3 *D*) (i.e., receptor loss is 17% larger in agrin-deprived clusters *C*(*t*) than in agrin-exposed clusters *A*(*t*) over the 24-h period), indicating that the clustered receptors become more stable when they are exposed to focal agrin.

The fact that both *A*(*t*)/*B*(*t*) and *C*(*t*)/*D*(*t*) decrease with *B*(*t*) and *D*(*t*) constants means that clustered AChRs are less stable than diffuse AChRs (whether they are exposed to agrin or not). This finding counters the intuition that clustered receptors, being more tightly associated, should be more stable than nonclustered ones. Also, the agrin-caused difference between *A*(*t*)/*B*(*t*) and *C*(*t*)/*D*(*t*) cannot be attributed to changes in absolute *B*(*t*) or *D*(*t*) (which stay fairly constant; see Fig. 3 *B*). Indeed, the plots in Fig. 3 *D* show how agrin significantly increases the stability of clustered AChRs (*A*(*t*)/*C*(*t*) increases) but does not have a significant effect on diffuse AChRs (*B*(*t*)/*D*(*t*) ~ ct.). Since *B*(*t*) and *D*(*t*) stay constant, we speculate that the likeliest route for AChR loss is directly in the direction orthogonal to the membrane (i.e., diffusive loss of receptors from cluster to noncluster areas is minimal or very local).

Agrin increases AChR addition into preexisting clusters

To measure AChR addition, we relabeled the AChRs with BTX* after $t = 24$ h (*vertical green arrow* in Fig. 2 *D* and in Fig. 3 graphs) and imaged at $t = 25$ h; the two time points are sufficiently close in time that the increase represents mainly the addition of new (nonlabeled) AChRs to the clusters (be it by insertion or by diffusion), i.e., we can safely neglect the receptor loss within that 1-h period (especially since, at this time, receptor loss has already slowed down significantly). Unfortunately, it was not possible to relabel with a different color-BTX* at the time, so insertion of new AChRs and diffusion of old AChRs could not be distinguished. The largest increases at $t = 25$ h (with respect to $t = 24$ h time-point values) were seen for *A*/*B* (9.9 ± 5.5%, maximum 16.3% in experiment 1) and for *A*/*C* (7.4 ± 5.0%, maximum 10.4% in experiment 1). *C*/*D* increases were an average of 5.2 ± 3.2%, and the lowest increase was *B*/*D* (1.8 ± 2.1%, with 0.5% reduction in experiment 1). In other words, despite the large fluctuations there is a clear trend $10\% \sim \Delta A/B > \Delta A/C > \Delta C/D > \Delta B/D \sim 0$. Thus, we can conclude that our 4-h focal application of agrin caused a statistically significant preferential addition of AChRs at clusters ($\Delta A/B$ and $\Delta A/C$ were largest) and small or no significant increase at the diffuse AChR areas ($\Delta B/D \sim 0$).

DISCUSSION

The focally stimulated myotube micropattern layout has several key advantages for studying AChR clustering over a homogeneously-stimulated, random myotube culture (where myotubes often overlap each other):

1. Single myotubes can be studied in isolation, avoiding confounding cell-cell contact interactions with other myotubes.
2. All the myotubes are straight and most of them of similar length (~1800 μm), and are stimulated with agrin at the same position relative to the myotube (albeit not with the same concentration at any given myotube position), thus avoiding confounding differences in cell-geometrical effects.
3. Each myotube and cluster can be easily found repeatedly during different imaging sessions as the cell culture is switched from the microscope to the incubator and back to the microscope.
4. Each experiment yields data on tens of myotubes simultaneously, providing rich statistics.
5. The spaces between myotubes provide a reference area for fluorescence background correction (see Image Analysis in Data S1and Fig. S2).

And, last but not least,

6. For any given myotube, it is possible to pick certain areas of the myotube as a reference to measure the fluorescence intensity in other areas.

Also, it is noteworthy that a random culture of myotubes has an unpredictable topology that induces chaotic mixing, which accelerates diffusive broadening of the focal stream (defeating the purpose of this study, data not shown); the orthogonal orientation used here minimizes the topologically induced enhanced mixing and allows for the focal stream to be at a constant position with respect to the microchannel walls.

Bruneau et al. has shown that innervated AChR clusters in mice are highly dynamic, with the AChRs continuously being degraded, inserted, and recycled (receptor recycling is turned off when synaptic activity is blocked) (32). In agreement with that work, our results suggest that AChR clusters should not be considered frozen aggregates of AChRs, as commonly depicted in textbooks, but instead, as boiling spots. These localized high turnover rates may reflect a cellular need for rapid synaptic reorganization that is particularly intense during synaptogenesis. At the central nervous system, a highly dynamic regulation of synaptic receptor density is known to be crucial for synaptic plasticity (see review (33)), so high receptor turnover may be a universal feature of synaptogenesis both in central nervous system and neuromuscular synapses. Our observations show that, at least in vitro, the cell directs its AChR removal and additional machinery with preference over the surrounding noncluster areas in response to a focal application of agrin, although agrin-predating clusters themselves may not be required for synaptogenesis if the nerve happens to hit an area that does not contain an aneural cluster (5). We postulate that, in this model, agrin acts as a molecular tag that tells this machinery when to slow down AChR loss and intensify AChR addition; the aggregation of aneural clusters continually provides innervation opportunities counteracting the AChR degradation/recycling mechanism that is essential for synaptic maintenance. Without agrin, loss overcomes addition and the cluster (if there to begin with) eventually disappears; with agrin, the balance between addition and loss is tipped in favor of AChR cluster survival. A thorough test of this hypothesis will require exploring a wider range of experimental conditions (e.g., several agrin doses) and competition experiments (i.e., more than one agrin stimulus per myotube). In vivo, the stabilizing effect of agrin might be cooperating with presynaptic and basal lamina interactions to precisely match the shape of AChR aggregates to the shape of the presynaptic branches (observed in mice (7) and Zebrafish (21)) before the onset of activity. Importantly, this action of agrin does not require neurotransmitter activity (unlike the previously described antideclustering role of agrin that counteracts the declustering action of ACh (7)). Preferential addition could occur either via an unknown targeted transport mechanism (insertion of newly-synthesized or recycled receptors (34)) or indirectly by conferring adhesiveness to AChRs so that clusters can constantly capture AChRs via in-membrane diffusion (30). (We emphasize that, in our system, some new microclusters form in the agrin-exposed areas (Fig. S4) that may eventually contribute to the larger, agrin-independent clusters.) Bruneau et al. (30) have used fluorescence recovery after photobleaching to show that lateral diffusion of AChRs may account only for ~9% of all AChRs accumulated in a given cluster within 8 h in myotubes not challenged with agrin; recovery of AChRs by lateral diffusion was even slower (twofold) when agrin was added to the myotube cultures. This is known to occur at mature postsynaptic AChR clusters in vivo (25). It has been proposed that the scaffolding protein rapsyn, which links AChRs to the cytoskeleton (35) and reduces degradation of AChRs when the stoichiometry of rapsyn to AChR is increased (36,37), may intervene in the stabilization of AChRs by agrin.

Our finding that focal application of agrin increases AChR addition to preexisting clusters agrees with previous findings only partially. If addition by diffusion were negligible (although it has been observed in C2C12 cultures accounting for 9% of AChR density recovery over 8 h (30)), our observation would be in agreement with an earlier finding (not using agrin) that AChR clusters display higher AChR insertion rates than nonclustered AChRs (31). On the other hand, Bruneau et al. (30) have studied AChR insertion (by relabeling with different colors) in C2C12 myotubes expressing protosynapse clusters upon agrin bath application and found that AChRs insert mostly at noncluster locations (i.e., forming new microclusters); in comparison, we also see such focal-agrin-induced microclusters upon relabeling at 25 h (*white arrows* in Fig. S4), but addition is favored at clustered locations and at agrin-exposed locations, i.e., $\Delta A/B$ and $\Delta A/C$ are the largest increases. Experiments with two-color relabeling are underway to determine the relative contributions of diffusion of old AChRs and insertion of new AChRs in focal agrin-induced addition of AChRs at protosynaptic clusters.

The clusters did not regain their initial density as shown by relabeling with BTX* at the end of 25-h experiments, possibly reflecting that the clusters are in the process of disassembly. The drop in AChR density after the first 25 h (21 h after removal of focal agrin) is consistent with a previous finding that found complete dissipation of agrin-independent clusters in C2C12 myotubes within 24 h after agrin (bath) withdrawal (34). Clusters lose AChRs primarily because AChRs are continuously targeted for degradation, but they can also spontaneously diffuse laterally away from the clusters. (In vivo, some are recycled back into the membrane, but Bruneau and Akaaboune have shown that there is no recycling of AChRs in C2C12 myotube cultures (34).) Clusters incorporate primarily newly-synthesized AChRs, but can also gain some by lateral diffusion from adjacent membrane regions: in C2C12 myotubes cultured on laminin, ~9% recovery by lateral diffusion in 8 h has been observed (30). The reason that in our experiments we do not see full recovery of the agrin-exposed clusters after relabeling may also be attributable to a suboptimal choice of agrin dose (as the physiological dose is not known, we chose one previously used in the literature) that only produces partial effects, and/or to the lack of other signals from the axon tip that are not present in the agrin stream. Future experiments are planned to find the agrin doses and other cell culture protocols that optimize the stability of protosynaptic AChRs.

Our microfluidic platform is similarly applicable to studies of spatiotemporal competition between different focal stimuli (several positions, onsets, and/or doses), exploring the role of agrin as well as other factors involved in synaptogenesis such as neuregulin and ACh.

SUPPLEMENTARY MATERIAL

To view all of the supplemental files associated with this article, visit www.biophysj.org.

The authors are grateful to Drs. Marv Adams, Stanley Froehner, and Lisa F. Horowitz for insightful comments and Dr. Greg Cooksey for assistance in image analysis.

This work was funded by the National Institute of Biomedical Imaging and Bioengineering under grant No. R01-EB001474.

REFERENCES

1. Cohen-Cory, S. 2002. The developing synapse: construction and modulation of synaptic structures and circuits. *Science*. 298:770–776.
2. Kandel, E. R., J. H. Schwartz, and T. M. Jessel. 2000. The formation and regeneration of synapses. *In* Principles of Neural Science. E. R. Kandel, J. H. Schwartz, and T. M. Jessel, editors. McGraw-Hill, New York.
3. Dai, Z., and H. B. Peng. 2001. Fluorescent imaging of nicotinic receptors during neuromuscular junction development. *In* Ion Channel Localization: Methods and Protocols. A. N. Lopatin and C. G. Nichols, editors. Humana Press, Totowa, NJ.
4. Anderson, M. J., and M. W. Cohen. 1977. Nerve-induced and spontaneous redistribution of acetylcholine receptors on cultured muscle cells. *J. Physiol.* 268:757–773.
5. Lin, S., L. Landmann, M. A. Ruegg, and H. R. Brenner. 2008. The role of nerve- versus muscle-derived factors in mammalian neuromuscular junction formation. *J. Neurosci.* 28:3333–3340.
6. Frank, E., and G. D. Fischbach. 1979. Early events in neuromuscular junction formation in vitro: induction of acetylcholine receptor clusters in the postsynaptic membrane and morphology of newly formed synapses. *J. Cell Biol.* 83:143–158.
7. Misgeld, T., T. T. Kummer, J. W. Lichtman, and J. R. Sanes. 2005. Agrin promotes synaptic differentiation by counteracting an inhibitory effect of neurotransmitter. *Proc. Natl. Acad. Sci. USA.* 102:11088–11093.
8. Flanagan-Steet, H., M. A. Fox, D. Meyer, and J. R. Sanes. 2005. Neuromuscular synapses can form in vivo by incorporation of initially aneural postsynaptic specializations. *Development.* 132:4471–4481.
9. Wang, Z. Z., A. Mathias, M. Gautam, and Z. W. Hall. 1999. Metabolic stabilization of muscle nicotinic acetylcholine receptor by rapsyn. *J. Neurosci.* 19:1998–2007.
10. McMahan, U. J. 1990. The agrin hypothesis. *Cold Spring Harb. Symp. Quant. Biol.* 55:407–418.
11. Sanes, J. R., and J. W. Lichtman. 1999. Development of the vertebrate neuromuscular junction. *Annu. Rev. Neurosci.* 22:389–442.
12. Bromann, P. A., H. Zhou, and J. R. Sanes. 2004. Kinase- and rapsyn-independent activities of the muscle-specific kinase (MuSK). *Neuroscience.* 125:417–426.
13. Cornish, T., D. W. Branch, B. C. Wheeler, and J. T. Campanelli. 2002. Microcontact printing: a versatile technique for the study of synaptogenic molecules. *Mol. Cell. Neurosci.* 20:140–153.
14. Tourovskaia, A., X. Figueroa-Masot, and A. Folch. 2006. Long-term microfluidic cultures of myotube microarrays for high-throughput focal stimulation. *Nat. Protocols.* 1:1092–1104.
15. Tourovskaia, A., X. Figueroa-Masot, and A. Folch. 2005. Differentiation-on-a-chip: a microfluidic platform for long-term cell culture studies. *Lab Chip.* 5:14–19.
16. Tourovskaia, A., T. F. Kosar, and A. Folch. 2006. Local induction of acetylcholine receptor clustering in myotube cultures using microfluidic application of agrin. *Biophys. J.* 90:2192–2198.
17. Kosar, T. F., A. Tourovskaia, X. Figueroa-Masot, M. E. Adams, and A. Folch. 2006. A nanofabricated planar aperture as a mimic of the nerve-muscle contact during synaptogenesis. *Lab Chip.* 6:632–638.
18. Yang, X., S. Arber, C. William, L. Li, Y. Tanabe, T. M. Jessell, C. Birchmeier, and S. J. Burden. 2001. Patterning of muscle acetylcholine receptor gene expression in the absence of motor innervation. *Neuron.* 30:399–410.
19. Lin, W., R. W. Burgess, B. Dominguez, S. L. Pfaff, J. R. Sanes, and K. F. Lee. 2001. Distinct roles of nerve and muscle in postsynaptic differentiation of the neuromuscular synapse. *Nature.* 410:1057–1064.
20. Pun, S., M. Sigrist, A. F. Santos, M. A. Ruegg, J. R. Sanes, T. M. Jessell, S. Arber, and P. Caroni. 2002. An intrinsic distinction in neuromuscular junction assembly and maintenance in different skeletal muscles. *Neuron.* 34:357–370.
21. Panzer, J. A., Y. Song, and R. J. Balice-Gordon. 2006. In vivo imaging of preferential motor axon outgrowth to and synaptogenesis at prepatterned acetylcholine receptor clusters in embryonic Zebrafish skeletal muscle. *J. Neurosci.* 26:934–947.
22. Tourovskaia, A., T. Barber, B. Wickes, D. Hirdes, B. Grin, D. Castner, K. E. Healy, and A. Folch. 2003. Micropatterns of chemisorbed cell adhesion-repellent films using oxygen plasma etching and elastomeric masks. *Langmuir.* 19:4754–4764.
23. Kummer, T. T., T. Misgeld, J. W. Lichtman, and J. R. Sanes. 2004. Nerve-independent formation of a topologically complex postsynaptic apparatus. *J. Cell Biol.* 164:1077–1087.
24. Tanford, C. 1961. Physical Chemistry of Macromolecules. Wiley, New York.
25. Akaaboune, M., R. M. Grady, S. Turney, J. R. Sanes, and J. W. Lichtman. 2002. Neurotransmitter receptor dynamics studied in vivo by reversible photo-unbinding of fluorescent ligands. *Neuron.* 34:865–876.

26. Chen, H., E. Rhoades, J. S. Butler, S. N. Loh, and W. W. Webb. 2007. Dynamics of equilibrium structural fluctuations of apomyoglobin measured by fluorescence correlation spectroscopy. *Proc. Natl. Acad. Sci. USA.* 104:10459–10464.

27. Andres, V., and K. Walsh. 1996. Myogenin expression, cell cycle withdrawal, and phenotypic differentiation are temporally separable events that precede cell fusion upon myogenesis. *J. Cell Biol.* 132:657–666.

28. Neville, C., N. Rosenthal, M. McGrew, N. Bogdanova, and S. Hauschka. 1997. Skeletal muscle cultures. *Methods Cell Biol.* 52:85–116.

29. Gesemann, M., A. J. Denzer, and M. A. Ruegg. 1995. Acetylcholine receptor-aggregating activity of agrin isoforms and mapping of the active site. *J. Cell Biol.* 128:625–636.

30. Bruneau, E. G., P. C. MacPherson, D. Goldman, R. I. Hume, and M. Akaaboune. 2005. The effect of agrin and laminin on acetylcholine receptor dynamics in vitro. *Dev. Biol.* 288:248–258.

31. Bursztajn, S., S. A. Berman, J. L. McManaman, and M. L. Watson. 1985. Insertion and internalization of acetylcholine-receptors at clustered and diffuse domains on cultured myotubes. *J. Cell Biol.* 101: 104–111.

32. Bruneau, E., D. Sutter, R. I. Hume, and M. Akaaboune. 2005. Identification of nicotinic acetylcholine receptor recycling and its role in maintaining receptor density at the neuromuscular junction in vivo. *J. Neurosci.* 25:9949–9959.

33. Malinow, R., and R. C. Malenka. 2002. AMPA receptor trafficking and synaptic plasticity. *Annu. Rev. Neurosci.* 25:103–126.

34. Bruneau, E. G., and M. Akaaboune. 2006. The dynamics of recycled acetylcholine receptors at the neuromuscular junction in vivo. *Development.* 133:4485–4493.

35. Phillips, W. D., D. Vladeta, H. Han, and P. G. Noakes. 1997. Rapsyn and agrin slow the metabolic degradation of the acetylcholine receptor. *Mol. Cell. Neurosci.* 10:16–26.

36. Gervasio, O. L., and W. D. Phillips. 2005. Increased ratio of rapsyn to ACh receptor stabilizes postsynaptic receptors at the mouse neuromuscular synapse. *J. Physiol.* 562:673–685.

37. Gervasio, O. L., P. F. Armson, and W. D. Phillips. 2007. Developmental increase in the amount of rapsyn per acetylcholine receptor promotes postsynaptic receptor packing and stability. *Dev. Biol.* 305: 262–275.